

## Tunneling Ionization Time Resolved by Backpropagation

Hongcheng Ni, Ulf Saalmann, and Jan-Michael Rost

Max-Planck-Institut für Physik komplexer Systeme, Nöthnitzer Strasse 38, 01187 Dresden, Germany

(Received 29 January 2016; published 8 July 2016)

We determine the ionization time in tunneling ionization by an elliptically polarized light pulse relative to its maximum. This is achieved by a full quantum propagation of the electron wave function forward in time, followed by a classical backpropagation to identify tunneling parameters, in particular, the fraction of electrons that has tunneled out. We find that the ionization time is close to zero for single active electrons in helium and in hydrogen if the fraction of tunneled electrons is large. We expect our analysis to be essential to quantify ionization times for correlated electron motion.

DOI: 10.1103/PhysRevLett.117.023002

Advances in laser technology have led to the generation of ultrashort intense laser pulses, whose time duration is in the range of the natural time scale of electron dynamics, rendering the observation and even control of electron dynamics in atoms and molecules possible [1,2]. Among them, the attoclock [3] is a powerful angular streaking (or mapping) technique to study attosecond electron dynamics using an elliptically polarized short infrared laser pulse. Depending on the instant of ionization, the photoelectron is deflected by the laser pulse to different directions.

Since for such intense-field experiments, the electron is dominantly released by tunneling ionization through the potential barrier formed by the combined potential of Coulomb attraction and dipole coupling to the light, it is tempting to use the attoclock for measuring tunneling ionization time in analogy to photoionization time measured in experiments combining a phase locked short attosecond pulse (for photoionization) with its generating infrared pulse (for timing the photoelectron) [4–6]. Indeed, experiments have been carried out to find the tunneling ionization time [3] and position [7]. Conceptually, however, these tunneling-ionization-time experiments differ from those for photoionization: In the latter, a relative phase  $\phi$  of the wave function between ionization from two different orbitals can be experimentally determined. It could be shown that this phase is uniquely related to the photoionization time delay, essentially correcting the time  $\tau_\phi = d\phi/dE$  by removing the asymptotic contributions  $\tau_C$  of the photoelectron interacting with the light field.

In the attoclock experiments, the situation seems to be similar at a first glance but is in reality fundamentally different: The angle  $\theta$  of photoemission gives formally also a time when divided by the angular frequency,  $\tau_\theta = \theta/\omega$ . Also here, one can, in principle, determine the asymptotic correction  $\tau_C$ . However, for interpreting  $\tau_\theta$ , it remains unclear which conditions for the electron one should associate with the reference angle, the minor polarization axis. More generally speaking, one has to formulate tunneling in this time-dependent problem which is not

directly linked to an observable. Several proposals have been put forward based on semiclassical reasoning [3,7,8] including complex variables [9] using an analytical  $R$ -matrix method [10,11], and the Feynman path integral assuming a static potential [12,13]. Common to these approaches is the extraction of a time by (i) approximating the actual electron dynamics and (ii) employing the explicit asymptotic correction  $\tau_C$ .

In the following, we propose an approach which neither needs (i) nor (ii): We calculate the wave function  $\Psi$  for an atom exposed to a short circularly polarized laser field by propagating the time-dependent Schrödinger equation (TDSE) numerically with the initial condition of the bound electron. At a time  $t'$  after the laser pulse (we check that the results do not depend on the specific value of  $t'$ ), we subtract the ground-state wave function to get  $\psi(\mathbf{r}') \equiv R(\mathbf{r}')\exp[iS(\mathbf{r}')] ]$ , such that  $\int |\psi|^2 d\mathbf{r}' = P_{\text{ion}}$  is the (quantum) ionization probability (atomic units are used unless stated otherwise). With the local momentum  $\nabla S(\mathbf{r}')$  [14,15], we propagate the resulting phase-space density  $\rho(\mathbf{p}', \mathbf{r}') = |\psi(\mathbf{r}')|^2 \delta(\mathbf{p}' - \nabla S(\mathbf{r}'))$  backwards with classical trajectories  $(\mathbf{p}(t), \mathbf{r}(t))$  subject to a criterion  $\Pi$  for tunneling ionization, which results in a distribution of tunneling ionization times  $\tau$ ,

$$\frac{d\mathcal{P}}{d\tau} = \int d\mathbf{r}' \Pi(\mathbf{p}, \tau) |\psi(\mathbf{r}')|^2. \quad (1)$$

The criterion that the electron has tunneled at time  $\tau$  if the kinetic momentum  $\mathbf{p} + \mathbf{A}$  in the instantaneous field direction  $\mathbf{F}$  vanishes,

$$\Pi(\mathbf{p}, \tau) = |\mathbf{p} + \mathbf{A}| |\mathbf{F}| \delta((\mathbf{p} + \mathbf{A}) \cdot \mathbf{F}) \delta(t - \tau), \quad (2)$$

captures adiabatic as well as nonadiabatic tunneling dynamics. We define the electric field  $\mathbf{F}(t) = -d\mathbf{A}/dt$  of the light pulse via the vector potential

$$\mathbf{A}(t) = \frac{A_0}{\sqrt{\varepsilon^2 + 1}} \cos^4(\omega t/2N) \begin{pmatrix} \cos(\omega t) \\ \varepsilon \sin(\omega t) \end{pmatrix} \quad (3)$$

with ellipticity parameter  $\varepsilon$  and angular frequency  $\omega$ . The pulse length is parametrized with the number of optical cycles  $N$  and  $\mathbf{A}$  vanishes for  $|t| \geq N\pi/\omega$ . Note that  $t = 0$  corresponds to the pulse center. The Hamiltonian used in both the classical and quantum propagations reads

$$H = \frac{1}{2}(\mathbf{p} + \mathbf{A}(t))^2 + V(r), \quad (4)$$

where for helium, we implement a single-active-electron (SAE) potential  $V(r)$  [16] and a soft core with  $r$  replaced by  $\sqrt{r^2 + a^2}$ . With  $a^2 = 0.19633$ , the ground state obtained through imaginary-time propagation has an energy of  $E_0 = -0.903577$ , close to the ionization potential of helium.

To obtain the ionized wave packet, we use the split-step Fourier method (or Fourier grid method) to numerically solve the TDSE  $(i\frac{\partial}{\partial t} - H)\Psi(\mathbf{r}, t) = 0$  on a grid with 9000 points in each dimension, a grid step of 0.2, and a time step of 0.02. In the simulations throughout the Letter, we use a two-cycle ( $N = 2$ ) circularly polarized ( $\varepsilon = 1$ ) laser pulse with a central wavelength of 800 nm. We employ absorbing boundaries of the form  $\cos^{1/6}[(\pi/2)(|x - x_0|/L)]$  over a width  $L$  in each direction for  $|x| \geq |x_0|$ . The boundary is chosen to span 10% of the grid size in each direction. We stop the simulations after the laser pulse and before the respective part of the wave packet has reached the boundary.

The backpropagation performed with classical trajectories [17] under the same Hamiltonian (4) automatically accounts for the Coulomb correction. When criterion (2) identifying a tunneling process is fulfilled for a trajectory  $j$ , the latter is stopped at that time  $\tau_{jk}$ . Typically, condition (2) is fulfilled for several times  $\tau_{jk}$  ( $k = 1, 2, \dots$ ) along a trajectory  $j$ , and we identify the event closest to the ion as the tunnel exit  $r_j(\tau_j) = \min_k \{r_j(\tau_{jk})\}$  to assign the weight  $|\psi(\mathbf{r}'_j, t')|^2$  of trajectory  $j$  to the tunneling probability at  $\tau_j$ .

The resulting distribution (1) for  $\tau$ , the tunneling ionization time (TIT) shown in Fig. 1, resembles closely the shape of the well-known tunneling ionization rates. The shape is a direct consequence of tunneling and essentially independent of the dimensionality of the problem. More details regarding the tunneling process can be obtained from the TIT distribution differential in space as provided in Fig. 2. The projections demonstrate that the probability distribution constructed with Eq. (1) exhibits indeed the typical features associated with a tunneling, namely, a correlation of the maximal field strength and its spatial position with the maximal ionization probability and the tunnel exit. Snapshots at three TITs during the pulse in Fig. 2(d) reveal

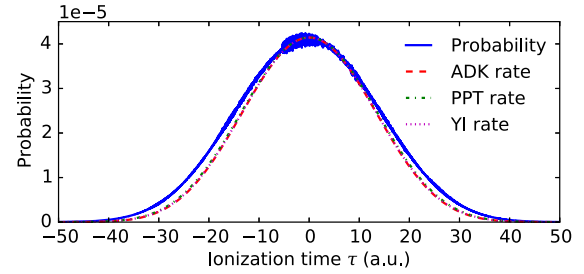


FIG. 1. Distribution (1) of tunneling ionization times [blue solid line, Eq. (1)] for ionization of a SAE helium atom with a laser pulse of  $8 \times 10^{14}$  W/cm<sup>2</sup> peak intensity as described in the text. In comparison, we show related instantaneous rates. For ADK [18,19], we use Eq. (9) of Ref. [19], for PPT [20–23] the equations summarized by Popov [23] [Eqs. (3.4)–(3.6)], and for YI the circular case in Yudin and Ivanov [24] [Eqs. (19) and (20)]. All rates are scaled to agree at the maximum.

that the tunnel exit follows essentially adiabatically the direction of the laser field, with a slight lag for its larger values.

We can integrate the distribution of the tunnel exits in Fig. 2(c) to give the distribution as a function of distance  $r$  from the ion or angle  $\theta$  in the polarization plane. The radial distribution Fig. 3(a) peaks sharply a bit closer to the ion than the static tunnel exit  $r_{\text{stat}}$  (dashed line) determined from the standard adiabatic potential at maximum field strength, sometimes also called the “field-direction model” [7]. This observation in line with the results from the model developed in Ref. [25] is rooted in the absorption of energy of the electronic wave packet from the laser pulse while traveling to the tunnel exit, i.e., a consequence of the

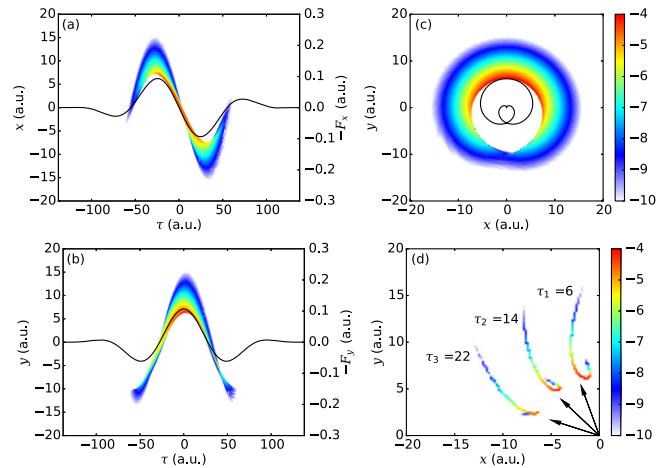


FIG. 2. Distributions  $d^3\mathcal{P}/drd\tau$  (in logarithmic scale) of the tunneling ionization time  $\tau$  and position  $(x, y)$  according to Eq. (1) for the system as in Fig. 1 projected onto the planes (a)  $\tau$ - $x$ , (b)  $\tau$ - $y$ , (c)  $x$ - $y$ , respectively, and (d) sliced at times  $\tau_i$  as indicated. Black lines or arrows indicate the electric field at times  $t = \tau$ , (a)  $-F_x$  (in a.u.), (b)  $-F_y$  (in a.u.), (c) and (d)  $-F$  (in arb. units).

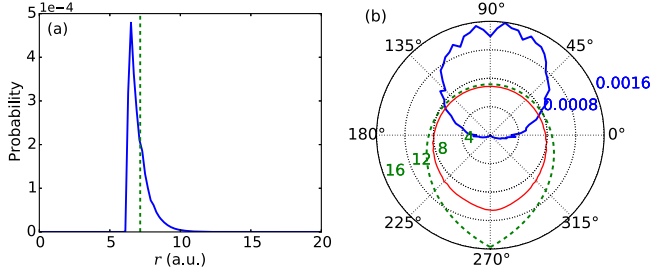


FIG. 3. Electron distributions (blue solid line) as in Fig. 2 but integrated over  $\tau$  and all phase-space variables but (a) the distance  $r$  to the ion and (b) the angle  $\theta$  in the polarization plane. The green dashed lines represent the respective static tunnel exit  $r_{\text{stat}}$ . Additionally shown in (b) is the angular distribution of mean tunnel exits from backpropagation (red solid line).

nonadiabaticity of the tunneling dynamics. Indeed, we find that the mean energy of the tunneled wave packet is slightly above the ground-state energy (not shown).

The angle-resolved tunnel-exit distribution [blue line in Fig. 3(b)] confirms that the electrons most probably tunnel out in the  $+y$  direction, as already seen in Fig. 2(c). The corresponding mean tunnel exits (red solid line) are compared again to the static ones (green dashed line). They vary with angle because the laser field has different amplitude in different directions [black line in Fig. 2(c)]. Our tunnel-exit positions are closer to the ion than the static ones for all angles. One also sees that in the direction of the maximum field ( $\theta = \pi/2$ ) the tunnel-exit positions have the smallest values in accordance with a tunneling scenario. One may take our results obtained from classical backpropagation of the full quantum solution as a quantitative confirmation of the standard tunneling models [18–24], most relevant for calculating electron momentum spectra.

Since our ionization is described fully quantum mechanically, we can quantify the range of validity of this tunneling picture. The tunneling probability  $P_{\text{tun}} = \int d\tau \mathcal{P}(\tau)$  of Eq. (1) consists of all trajectories which have stopped according to the criterion (2) upon classical backpropagation. Consequently,

$$\chi = (P_{\text{ion}} - P_{\text{tun}})/P_{\text{ion}} \quad (5)$$

is a measure for the fraction of ionization not accounted for by the tunneling scenario. We show  $\chi$  in Fig. 4 as a function of laser peak intensity  $I$  along with the mean tunneling ionization time  $\langle \tau \rangle = \int d\tau \tau d\mathcal{P}/d\tau$ . One sees that around  $I = 2 \times 10^{14} \text{ W/cm}^2$   $\langle \tau \rangle$  is close to zero and slightly decreases for larger intensities due to depletion of the ground state [9]. For all these intensities,  $\chi$  is very small and the tunneling scenario applies. However, for  $I < 1.5 \times 10^{14} \text{ W/cm}^2$ , the fraction of nontunneled ionization events  $\chi$  is no longer negligible since the multiphoton regime is approached (compare the Keldysh parameter given on the top axis). Not surprisingly,  $\langle \tau \rangle$  changes rapidly, which

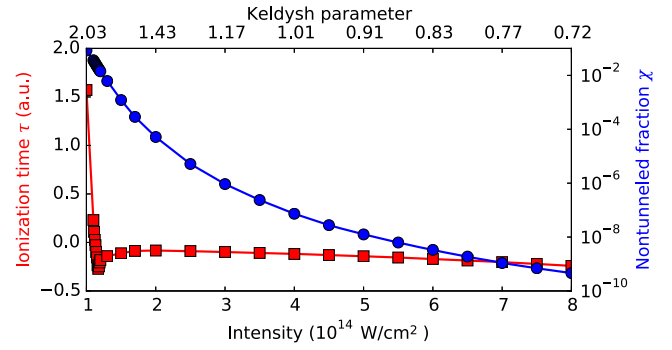


FIG. 4. The fraction of nontunneled electron probability  $\chi$  (blue circles) according to Eq. (5) and the mean tunneling ionization time (red squares) for helium as in Fig. 1.

indicates a breakdown of the tunneling picture whose validity is necessary to interpret  $\langle \tau \rangle$  the way it is constructed as the tunneling ionization time.

This close-to-zero tunneling ionization time at higher intensities obtained after the Coulomb correction is accounted for by backpropagation is similar to the situation of time delays in photoionization [26,27] and nonresonant two-photon ionization [28]. In this context, the photo-absorption time delay turns out to be zero after separation from the continuum time delay.

For helium in the  $10^{14} \text{ W/cm}^2$  intensity range, we have only seen the limitation of the tunneling scenario towards lower intensities. With a weaker bound system such as hydrogen, we expect to see the tunneling scenario limited also towards higher intensities due to the (nonclassical) behavior of the electron dynamics close to the (adiabatic) barrier top. This is indeed the case, as Fig. 5 reveals. We see (red squares) for small intensities  $\langle \tau \rangle \approx 0$  in agreement with the results from Ref. [9] (red dashed line) but a dramatic change around  $I = 2.5 \times 10^{14} \text{ W/cm}^2$  where the fraction of nontunneled ionization contributions  $\chi$  (blue circles) increases suddenly due to close and even over-the-barrier dynamics. Note that the saddle-point technique used in

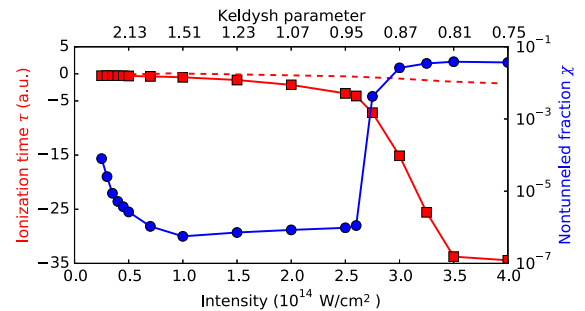


FIG. 5. The fraction of nontunneled ionization probability  $\chi$  (blue circles) according to Eq. (5) and the mean tunneling ionization time (red squares) as in Fig. 4 but for hydrogen with potential  $V(r) = -(r^2 + 0.63629)^{-1/2}$ . The red dashed curve is the ionization time from Ref. [9].

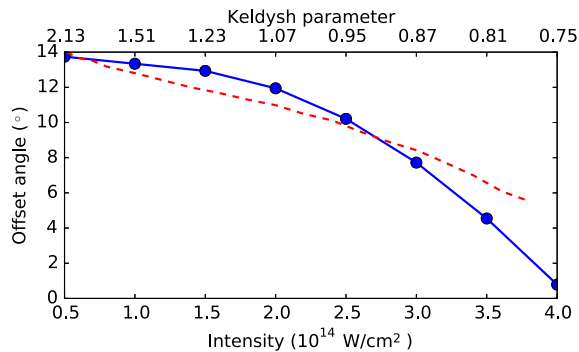


FIG. 6. Intensity dependence of the electron emission angle perpendicular to the direction of maximal field strength of the light pulse for hydrogen as in Fig. 5. The red dashed curve is the corresponding angle from Ref. [9].

Ref. [9] precludes a description of the transition to over-barrier ionization. Consequently, in this description,  $\langle\tau\rangle$  remains close to zero once corrected for depletion. Note that substantial depletion indicates a loss of the connection of dominant ionization around the laser field maximum, which is a prerequisite for the original idea of the attoclock.

A little thought reveals that the change from tunneling to over-barrier ionization should have much less effect on the (observable) photoemission angle  $\theta$  of the attoclock than on  $\langle\tau\rangle$  since  $\theta$  will be linked to the direction of maximum field strength also above the barrier as confirmed by the calculated attoclock angles for hydrogen in Fig. 6. One sees fairly good agreement even between our 2D calculation and the 3D calculation from Ref. [9].

In conclusion, through classical backpropagation of a (quantum-mechanically) ionized electron wave packet, we have been able to determine to which extent the electron has been released through tunneling. If the tunneling scenario applies, we have found for a single active electron the tunneling ionization time to be close to zero in accordance with previous findings [9]. Thereby, we also have been able to confirm the ionization rates from well-accepted tunneling approaches such as the ADK and PPT theories.

The classical backpropagation naturally corrects for possible phase (time) delays through interaction of the ionized electron with the light pulse on the way to the detector. Moreover, its generality allows one to reformulate other approaches [25,29–34] in terms of an appropriate projector  $\Pi$  and, therefore, enables comparison on the same footing. Most important, however, the classical backpropagation of a quantum-mechanically determined ionization probability allows one to determine quantitatively the fraction of nontunneled electrons, since our tunneling analysis does not modify the (quantum-mechanically calculated) ionization yield. If this fraction is close to zero, one may safely associate the ionization times with the tunneling process. Quantifying the tunneling character of ionization dynamics as introduced here shows a route to determine

tunneling ionization times reliably in systems with two or more electrons.

H. N. would like to thank A. S. Landsman, C. Hofmann, N. Takemoto, and Q. C. Ning for helpful discussions. This work was supported by Alexander von Humboldt Foundation.

- 
- [1] F. Krausz and M. Ivanov, *Rev. Mod. Phys.* **81**, 163 (2009).
  - [2] T. Popmintchev, M.-C. Chen, P. Arpin, M. M. Murnane, and H. C. Kapteyn, *Nat. Photonics* **4**, 822 (2010).
  - [3] P. Eckle, M. Smolarski, P. Schlup, J. Biegert, A. Staudte, M. Schöffler, H. G. Muller, R. Dörner, and U. Keller, *Nat. Phys.* **4**, 565 (2008).
  - [4] M. Schultz *et al.*, *Science* **328**, 1658 (2010).
  - [5] J. M. Dahlström, D. Guénot, K. Klünder, M. Gisselbrecht, J. Mauritsson, A. L’Huillier, A. Maquet, and R. Taïeb, *Chem. Phys.* **414**, 53 (2013).
  - [6] R. Pazourek, S. Nagele, and J. Burgdörfer, *Rev. Mod. Phys.* **87**, 765 (2015).
  - [7] A. N. Pfeiffer, C. Cirelli, M. Smolarski, D. Dimitrovski, M. Abu-samha, L. B. Madsen, and U. Keller, *Nat. Phys.* **8**, 76 (2012).
  - [8] M. Li, J.-W. Geng, H. Liu, Y. Deng, C. Wu, L.-Y. Peng, Q. Gong, and Y. Liu, *Phys. Rev. Lett.* **112**, 113002 (2014).
  - [9] L. Torlina, F. Morales, J. Kaushal, I. Ivanov, A. Kheifets, A. Zielinski, A. Scrinzi, H. G. Muller, S. Sukiasyan, M. Ivanov, and O. Smirnova, *Nat. Phys.* **11**, 503 (2015).
  - [10] L. Torlina and O. Smirnova, *Phys. Rev. A* **86**, 043408 (2012).
  - [11] L. Torlina, M. Ivanov, Z. B. Walters, and O. Smirnova, *Phys. Rev. A* **86**, 043409 (2012).
  - [12] A. S. Landsman, M. Weger, J. Maurer, R. Boge, A. Ludwig, S. Heuser, C. Cirelli, L. Gallmann, and U. Keller, *Optica* **1**, 343 (2014).
  - [13] A. S. Landsman and U. Keller, *J. Phys. B* **47**, 204024 (2014).
  - [14] B. Feuerstein and U. Thumm, *J. Phys. B* **36**, 707 (2003).
  - [15] X. Wang, J. Tian, and J. H. Eberly, *Phys. Rev. Lett.* **110**, 243001 (2013).
  - [16] X. M. Tong and C. D. Lin, *J. Phys. B* **38**, 2593 (2005).
  - [17] For propagation of phase-space distributions with classical trajectories, see J. M. Rost, *Phys. Rep.* **297**, 271 (1998).
  - [18] M. V. Ammosov, N. B. Delone, and V. P. Krainov, *Sov. Phys. JETP* **64**, 1191 (1986).
  - [19] N. B. Delone and V. P. Krainov, *Phys. Usp.* **41**, 469 (1998).
  - [20] A. M. Perelomov, V. S. Popov, and M. V. Terent’ev, *Sov. Phys. JETP* **23**, 924 (1966).
  - [21] A. M. Perelomov, V. S. Popov, and M. V. Terent’ev, *Sov. Phys. JETP* **24**, 207 (1967).
  - [22] A. M. Perelomov and V. S. Popov, *Sov. Phys. JETP* **25**, 336 (1967).
  - [23] V. S. Popov, *Phys. Usp.* **47**, 855 (2004).
  - [24] G. L. Yudin and M. Y. Ivanov, *Phys. Rev. A* **64**, 013409 (2001).
  - [25] M. Klaiber, K. Z. Hatsagortsyan, and C. H. Keitel, *Phys. Rev. Lett.* **114**, 083001 (2015).

- [26] J. Su, H. Ni, A. Becker, and A. Jaroń-Becker, *Phys. Rev. A* **88**, 023413 (2013); **89**, 013404 (2014).
- [27] J. Su, H. Ni, A. Becker, and A. Jaroń-Becker, *Chin. J. Phys.* **52**, 404 (2014).
- [28] J. Su, H. Ni, A. Jaroń-Becker, and A. Becker, *Phys. Rev. Lett.* **113**, 263002 (2014).
- [29] I. Barth and O. Smirnova, *Phys. Rev. A* **84**, 063415 (2011).
- [30] J. Kaushal and O. Smirnova, *Phys. Rev. A* **88**, 013421 (2013).
- [31] E. Yakaboylu, M. Klaiber, H. Bauke, K. Z. Hatsagortsyan, and C. H. Keitel, *Phys. Rev. A* **88**, 063421 (2013).
- [32] C. Hofmann, A. S. Landsman, A. Zielinski, C. Cirelli, T. Zimmermann, A. Scrinzi, and U. Keller, *Phys. Rev. A* **90**, 043406 (2014).
- [33] J.-W. Geng, L. Qin, M. Li, W.-H. Xiong, Y. Liu, Q. Gong, and L.-Y. Peng, *J. Phys. B* **47**, 204027 (2014).
- [34] N. Teeny, E. Yakaboylu, H. Bauke, and C. H. Keitel, *Phys. Rev. Lett.* **116**, 063003 (2016).